IEEE Access
Multidisciplinary ⋮ Rapid Review ⋮ Open Access Journal

Received July 16, 2020, accepted July 24, 2020, date of publication July 30, 2020, date of current version August 13, 2020.

Digital Object Identifier 10.1109/ACCESS.2020.3013124

Crosstalk-Based Test Setup Reproducing Radiated Susceptibility Effects in Wire Bundles

TAO LIANG[1], (Member, IEEE), XINGLONG WU[2], (Graduate Student Member, IEEE), FLAVIA GRASSI[2], (Senior Member, IEEE), GIORDANO SPADACINI[2], (Senior Member, IEEE), AND SERGIO AMEDEO PIGNARI[2], (Fellow, IEEE)

[1]State Key Laboratory of Electrical Insulation and Power Equipment, School of Electrical Engineering, Xi'an Jiaotong University, Xi'an 710049, China
[2]Department of Electronics, Information and Bioengineering, Politecnico di Milano, 20133 Milan, Italy

Corresponding author: Xinglong Wu (xinglong.wu@polimi.it)

ABSTRACT In the development of alternative test methods for pre-compliance radiated-susceptibility (RS) investigations, it is proven that a special test setup, involving an additional wire placed in proximity of the cable under test and fed by two radio-frequency generators, can reproduce through crosstalk (XT) the same terminal voltages/currents induced in the standard RS test setup, on condition that those generators are properly controlled in magnitude and phase. Such a test setup does not require expensive facilities like anechoic chambers and powerful amplifiers to feed antennas, therefore it represents a fast and cheap alternative to get feedback on radiated immunity in the early-design stage, before the formal RS assessment carried out according to standards. While in past literature works the equivalence between XT and RS was demonstrated for some simple cables like a single bare wire or a differential pair, this paper presents a new XT-based test setup suitable for the practically relevant case of a complex bundle of dielectric-covered wires. To this aim, two different formulations of feeding conditions are proposed, one more rigorous, based on multiconductor-transmission-line modeling, and one approximate, based on bundle-reduction techniques. The performance of both the equivalence schemes is assessed and discussed in the frequency range between 1 MHz and 1 GHz.

INDEX TERMS Crosstalk, electromagnetic compatibility, multiconductor transmission lines, radiated susceptibility.

I. INTRODUCTION

Along the path of electromagnetic-compatibility certifications that any industrial equipment must follow to get market-ready, proving compliance with radiated-susceptibility (RS) requirements is a notorious obstacle, owing to high costs of instrumentation, personnel and execution time [1]–[4]. Standard RS test procedures make use of high-power amplifiers to feed antennas in anechoic chambers, so to generate interfering electromagnetic fields impinging the equipment in operation. Often, unveiled malfunctions force designers to face challenging prototype reviews and iterative testing, needing continuous access to appropriate experimental facilities which are generally owned by specialized third-party labs. Therefore, the search for alternative test procedures, using simple test-bench setups, for faster and cheaper pre-compliance RS internal investigations at the early-design stage is of crucial interest for product designers.

In this respect, a number of possible testing strategies were developed in past years, and all of them were based on the fundamental observation that, for equipment enclosed in well-shielded cases, the dominant RS interference mechanism is coupling of radiated fields to external wiring harness (communications and/or power cables). In principle, equivalent effects could be reproduced by using appropriate coupling devices injecting radio-frequency (RF) currents directly into such wiring harness, and exploited to design time and cost effective pre-compliance test procedures.

Particularly, the theoretical and experimental comparisons between the currents induced by RS and injection were firstly provided in [5] and [6], respectively. The use of two bulk current injection (BCI) probes clamped on the cable harness interconnecting the units under test was investigated in [7]. This technique was further applied to reproduce electromagnetic pulse (EMP) tests in [8] and [9]. Though BCI

The associate editor coordinating the review of this manuscript and approving it for publication was Andrei Muller.

probes are effective coupling devices from the viewpoint of RF energy transfer, they perturb the passive characteristics of the test setup by inserting a lumped series impedance. As a consequence, proper RF feeding conditions ensuring equivalence with RS show complex frequency responses, which are dependent on many setup parameters, including the aforementioned series impedance and, even worse, the common-mode (CM) impedance of the equipment under test, which is normally unknown to operators. Only renouncing the deterministic reproduction of RS effects in favor of a relaxed statistical approach (that is, correlation of BCI and RS induced currents) can solve these problems.

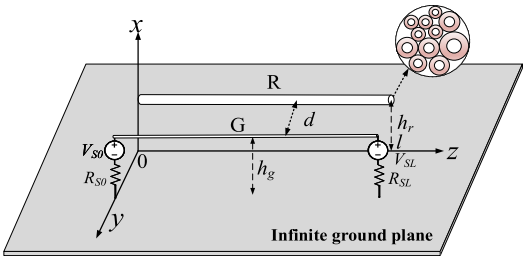

FIGURE 1. Principle drawing of the XT test setup used to reproduce FC-induced effects in the terminations of the cable harness.

Another promising alternative is to resort to crosstalk (XT) among wires as coupling mechanism [10], [11]. A principle drawing of the corresponding test setup is shown in Fig. 1, where interference is induced in the harness under test by placing in its close proximity an additional wire fed by two RF generators connected at the terminals. Unlike for BCI, the required feeding conditions do not depend on the terminal equipment (i.e., on the terminal impedances), thus assuring equivalence with the noise induced by RS even in the presence of non-linear loads. Such a solution, investigated so far for basic wiring structures only, [10], [11], is here investigated in the practical case of wiring harnesses composed of several coated wires, leading to two different approaches to enforce equivalence between the currents induced by RS and crosstalk.

The paper is organized as follows. Basic principles of the crosstalk-based RS tests are introduced in Section II. In Section III, exact conditions for equivalence are formulated by exploiting MTL models of the RS and XT test setup under analysis. Approximate conditions for equivalence are formulated in Section IV based on bundle reduction. Accuracy of the aforesaid exact and approximate conditions for equivalence is investigated by simulation in Section IV and Section V. Finally, conclusions are drawn in Section VI.

II. CROSSTALK-BASED RS TESTS

As schematically shown in Fig. 1, the crosstalk-based RS test setup involves an additional wire running parallel and in close proximity to the harness under test, which is driven by two RF sources connected at the terminations. Voltages and currents in such a *generator* wire induce interference through capacitive and inductive coupling into the cable under test. It is proven in [10] and [11] that appropriate feeding conditions (i.e., magnitude and phase of the two generators) can reproduce the same frequency response of currents/voltages induced in the equipment under test by a plane-wave electromagnetic field with arbitrary incidence and polarization. In these works, only canonical wiring structures, i.e., single-ended interconnections [10] and twisted wire pairs [11], were considered as harnesses under test, since the objective was to elaborate the basic principles of the test procedure. Conversely, in this work, enforcing equivalence between XT and RS is reformulated in order to tackle more realistic test setups, involving possibly complex wire bundles. As a result, two possible approaches, leading to corresponding sets of feeding conditions for the generator circuit, are developed.

In the first proposed method, rigorous equivalence between RS and XT is analyzed by modeling the wire bundle as a multiconductor-transmission line (MTL). It will be shown that RS effect (both the CM current of the bundle and individual currents of each wire) can be satisfactorily reproduced in the XT test setup, provided that two practical conditions called ''weak coupling'' and ''filament-bundle'' are satisfied. The expression of feeding conditions is obtained in closed form. It will be shown that, although equivalence is enforced for the CM only, the proposed scheme has also the potential to effectively reproduce the noise currents induced in individual wires in the bundle. The second, more approximate approach is based on bundle-reduction techniques [12]–[14] used to substitute the original MTL model with a CM-equivalent single-wire model, thus allowing reuse of the simple feeding conditions developed in [10].

III. EXACT CONDITIONS OF EQUIVALENCE

In this Section, a general scheme enforcing equivalence between XT and RS in terms of equal CM currents induced at the harness terminals is presented. The derivation makes use of MTL theory and to port-reduction in order to obtain an equivalent representation of the involved FC and XT test setups.

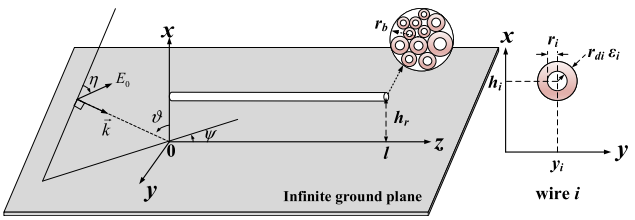

FIGURE 2. Principle drawing of the RS test setup under analysis.

A. FIELD-TO-WIRE COUPLING (FC) CIRCUIT MODEL

The cable harness shown in Fig. 2 is considered as the circuit subject to radiated interference. The harness is composed of n coated wires of length l, running at average height h_r above an ideal ground plane. As shown in the left panel of Fig. 2, positioning and characteristics of the i-th $(i = 1, 2, \ldots n)$

wire in the bundle are assigned by the following parameters: height above ground h_i, transversal displacement y_i, conductor radius r_i, dielectric thickness r_{di}, and dielectric permittivity ε_i. The radius of the overall bundle cross-section is denoted by r_b.

The interfering electromagnetic (EM) field, generated by an antenna in an anechoic environment, is approximated by a uniform plane wave characterized by elevation angle ϑ, azimuth angle ψ, polarization angle η, and electric-field strength E_0 [11]. Without loss of generality, since the objective here is to mimic typical incidence conditions foreseen by aerospace and automotive Standards, the azimuth angle is hereinafter set to the value $\psi = 90°$ (broadside incidence), and the polarization angle to the values $\eta = 0°$ and $\eta = 90°$ for vertical (VP) and horizontal (HP) polarization of the generating antenna, respectively. Moreover, based on the suggested distance and height of the phase center of the antenna with respect to the device under test in the standard, the elevation angle is set to the value $\vartheta = 73°$ [11], and a unitary electric-field strength $E_0 = 1$ V/m is considered as reference quantity. In order to predict induced quantities at the terminals of the cable structure under test, the general idea proposed in the literature [15], [16] is to use induced equivalent voltage or circuit sources to model the impact of FC.

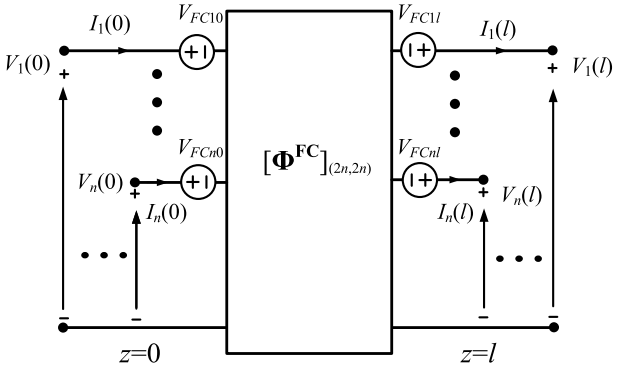

FIGURE 3. Equivalent circuit representation at the output ports of the RS test setup in Fig. 2.

Based on [14], an equivalent circuit representation (valid at the wire terminals) of the test setup in Fig. 2 is shown in Fig. 3, where the voltage-source vector $\mathbf{V_{FC0}} = [V_{FC10}, \cdots, V_{FCi0}, \cdots, V_{FCn0}]^T$, $\mathbf{V_{FCL}} = [V_{FC1l}, \cdots, V_{FCil}, \cdots, V_{FCnl}]^T$ account for the effects at the left ($z = 0$) and right ($z = l$) terminals due to the interfering EM field, respectively. For this $2n$-port network, the relationships between voltages and currents at the terminal ports are cast in matrix form as

$$\begin{bmatrix} \mathbf{V}(l) - \mathbf{V}_{\mathrm{FCL}} \\ \mathbf{I}(l) \end{bmatrix} = \mathbf{\Phi}^{\mathrm{FC}} \cdot \begin{bmatrix} \mathbf{V}(0) - \mathbf{V}_{\mathrm{FC0}} \\ \mathbf{I}(0) \end{bmatrix}, \tag{1}$$

where $\mathbf{V}(0)$, $\mathbf{V}(l)$ and $\mathbf{I}(0)$, $\mathbf{I}(l)$ are $n\times$ 1 vectors collecting voltages and currents on individual wires at the left (i.e., z = 0) and right (i.e., $z = l$) terminals, whereas $\mathbf{\Phi}^{\mathrm{FC}}$ denotes the $2n \times 2n$ chain parameter matrix associated with the cable bundle.

B. CROSSTALK (XT) CIRCUIT MODEL

In order for the noise induced by FC to be reproduced, a single-ended generator circuit (referred to as generator, G) is placed in close proximity and parallel to the cable axis, as shown in Fig. 1. Characteristics of the generator wire are the following: wire radius r_g, thickness and permittivity of dielectric jacket t_g and ε_g, respectively, distance from the cable axis d, height above ground h_g. According to the analysis in [10], the generator circuit is driven by two non-ideal voltage sources connected at both wire terminals, and characterized by open circuit voltages V_{S0}, V_{SL} and internal resistances R_{S0}, R_{SL}, respectively.

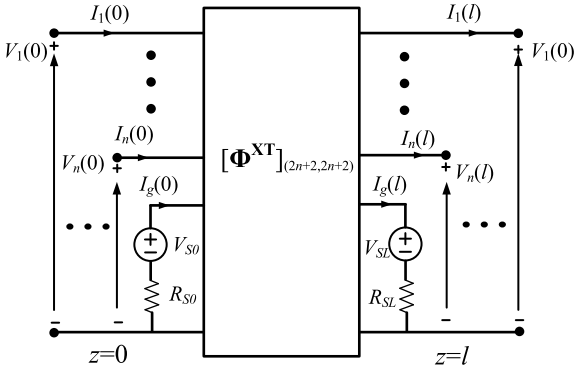

FIGURE 4. Principle drawing of the XT test setup in Fig. 1.

Resorting to MTL theory, the wiring structure involving the n wires in the bundle and the generator wire are modeled as a $2(n + 1)$-port network (see Fig. 4), whose voltages and currents at the terminations are related by

$$\begin{pmatrix} \mathbf{V}(l) \\ V_g(l) \\ \mathbf{I}(l) \\ I_g(l) \end{pmatrix} = \mathbf{\Phi}^{\mathrm{XT}} \cdot \begin{pmatrix} \mathbf{V}(0) \\ V_g(0) \\ \mathbf{I}(0) \\ I_g(0) \end{pmatrix} \tag{2}$$

where: $\mathbf{\Phi}^{\mathrm{XT}}$ is the $2(n+1) \times 2(n+1)$ chain parameter matrix associated with the $n+1$ wires in Fig. 1; $\mathbf{V}(0)$, $\mathbf{V}(l)$ and $\mathbf{I}(0)$, $\mathbf{I}(l)$ are $n \times 1$ vectors collecting voltages and currents at the terminations of individual wires in the bundle as in (1); $V_g(0)$, $V_g(l)$ and $I_g(0)$, $I_g(l)$ are voltages and currents at the left and right terminations of the generator wire, respectively.

Enforcing the port constraints $V_g(0) = V_{S0} - R_{S0}I_g(0)$ and $V_g(l) = V_{SL} - R_{SL}I_g(l)$ at the left and right terminations, respectively, of the generator wire, the passive $2(n + 1)$-port in Fig. 4 is converted (after some algebra here omitted for brevity) into the active $2n$-port shown in Fig. 5, whose chain-parameter representation:

$$\begin{bmatrix} \mathbf{V}(l) - \mathbf{V}_{\mathrm{XTL}} \\ \mathbf{I}(l) \end{bmatrix} = \mathbf{\Phi}_{\mathrm{eq}}^{\mathrm{XT}} \cdot \begin{bmatrix} \mathbf{V}(0) - \mathbf{V}_{\mathrm{XT0}} \\ \mathbf{I}(0) \end{bmatrix} \tag{3}$$

resembles the one cast for FC in (1).

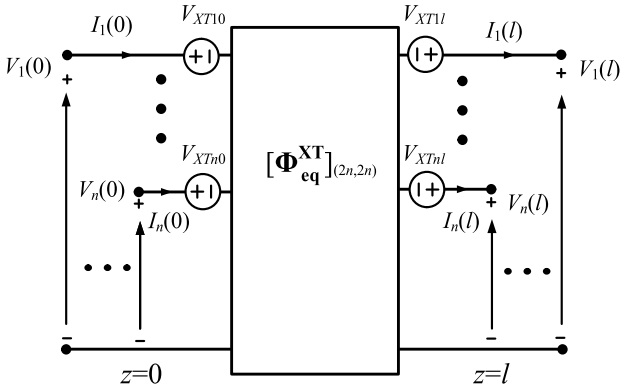

FIGURE 5. Equivalent representation at the output ports of the victim harness in Fig. 3, including active and passive effects due to the presence of the generator circuit.

The 2n-port network in Fig. 5 provides an equivalent representation of the original harness subject to XT coupling with the generator wire, and is valid for predicting voltages and currents induced by XT at the cable ends in spite of the specific terminal loads. Inclusion of the generator wire in the equivalent representation of the victim harness involves a twofold effect. Namely, the active part of the model, i.e., source vectors $\mathbf{V}_{\mathrm{XT0}} = [V_{XT\,10}, \cdots, V_{XTi0}, \cdots, V_{XTn0}]^T$ and $\mathbf{V}_{\mathrm{XTL}} = [V_{XT\,1l}, \cdots, V_{XTil}, \cdots, V_{XTnl}]^T$, represent the RF energy transfer from the generator wire to each wire in the victim harness. The passive part of the model, i.e., the $2n \times 2n$ chain-parameter matrix $\mathbf{\Phi}^{\mathrm{XT}}_{\mathrm{eq}}$, accounts for propagation effects along the cable harness, in the presence of a further wire (i.e., the generator wire) in close proximity. Hence, the entries of $\mathbf{\Phi}^{\mathrm{XT}}_{\mathrm{eq}}$ are expected to be generally different from those associated with the original bundle, i.e., entries of matrix $\mathbf{\Phi}^{\mathrm{FC}}$ in (1), due to the effect of perturbation of the original per-unit-length (p.u.l.) owing to the presence of the generator wire.

C. PREREQUISITES FOR EQUIVALENCE

By comparing the systems of equations in (1) and (3), two prerequisites to assure equivalence between FC and XT are identified as:

$$\mathbf{\Phi}^{\mathrm{FC}} \approx \mathbf{\Phi}^{\mathrm{XT}}_{\mathrm{eq}} \tag{4}$$

$$\mathbf{V}_{\mathrm{FC0}} \approx \mathbf{V}_{\mathrm{XT0}}, \quad \mathbf{V}_{\mathrm{FCL}} \approx \mathbf{V}_{\mathrm{XTL}}. \tag{5}$$

As previously stressed, the former condition in (4) requires the effect of perturbation introduced by the presence of the generator wire on the p.u.l. parameters of the victim harness to be negligible. As proven in [10] for a single-ended structure, such a condition is met as long as the generator wire and the wiring harness under test are weakly coupled, that is if a sufficient separation between them is assured. Since, a rigorous reformulation of the weak-coupling condition for complex wiring harnesses involving coated wires is not straightforward, in the remainder of this work the simplified condition $d \gg r_b$ will be exploited to ensure weak coupling, and the differences between the two matrices in (4) will be neglected as long as (rule of thumb) $d > 10\,r_b$.

The latter condition, (5), requires the voltage sources induced by FC and XT to be the same for every single wire in the bundle. However, the inherent difference between FC and XT coupling-mechanisms suggests that exact equivalence between all the corresponding induced sources is definitely hard to achieve. Hence, in order for the condition in (5) to be approximately satisfied, also the so-called "filament bundle" approximation (i.e., $h \gg r_b$) [17] is introduced, which allows neglecting spatial differences between the wires in the bundle, i.e., $h_i \approx h_r, y_i \approx 0$ for $i = 1, 2, \cdots, n$. For FC, the filament bundle approximation, which assumes equal induced voltages on all the line wires, leads to equal FC-induced sources, i.e., $V_{FCi0} \approx V_{FC0}$, $V_{FCil} \approx V_{FCl} \forall i$, (for bare-wire harnesses, a proof for filament bundle approximation can be found in [17]). A similar result, i.e., $V_{XTi0} \approx V_{XT0},$, $V_{XTil} \approx V_{XTl}$, $\forall i$, is obtained also for XT, on condition the filament bundle approximation (i.e., $h \gg r_b$) is combined with the assumption of weak coupling (i.e., $d \gg r_b$). For bare-wire structures, this property can be readily proven by recalling the analytical expressions of the mutual p.u.l. inductances and capacitances between the generator wire and the i-th wire in the bundle, i.e.,

$$L_{gi} = \frac{\mu_0}{4\pi} \ln\left(\frac{4h_g h_i}{s_{gi}^2}\right), \quad C_{gi} = 4\pi\varepsilon_0 \Big/ \ln\left(\frac{4h_g h_i}{s_{gi}^2}\right) \tag{6}$$

where μ_0, ε_0 denote free-space permeability and permittivity, respectively. By recognizing that: a) $h_i \approx h_r \ \forall i$, if $h \gg r_b$ (filament bundle approximation), and b) $s_{gi} \approx d \ \forall i$, if $d \gg r_b$ (weak coupling), the expressions in (6) show that inductive and capacitive coupling (proportional to L_{gi} and C_{gi}, respectively) between each wire in the bundle and the generator wire approximately take the same value, thus leading to nearly-equal XT-induced sources.

D. FEEDING CONDITIONS

To assure equivalence between the FC- and XT-induced sources as required by (5), the frequency response of the open-end voltage sources V_{S0}, V_{SL} connected at the terminations of the generator circuit shall be evaluated. This task can be accomplished analytically for canonical wiring structures in free space [10]. Conversely, in the presence of inhomogeneous media, numerical evaluation is required.

To this end, the submatrices $\mathbf{\Phi}_{kj}$, $k, j = 1, \ldots, 4$ and $\mathbf{\Phi}^{eq}_{m,n}$, $m, n = 1, 2$ are preliminary introduced, by partitioning the chain parameter matrices $\mathbf{\Phi}^{\mathrm{XT}}$, $\mathbf{\Phi}^{\mathrm{XT}}_{\mathrm{eq}}$, respectively, as:

$$\mathbf{\Phi}^{\mathrm{XT}} = \begin{bmatrix} [\mathbf{\Phi}_{11}]_{n\times n} & [\mathbf{\Phi}_{12}]_{n\times 1} & [\mathbf{\Phi}_{13}]_{n\times n} & [\mathbf{\Phi}_{14}]_{n\times 1} \\ [\mathbf{\Phi}_{21}]_{1\times n} & \Phi_{22} & [\mathbf{\Phi}_{23}]_{1\times n} & \Phi_{24} \\ [\mathbf{\Phi}_{31}]_{n\times n} & [\mathbf{\Phi}_{32}]_{n\times 1} & [\mathbf{\Phi}_{33}]_{n\times n} & [\mathbf{\Phi}_{34}]_{n\times 1} \\ [\mathbf{\Phi}_{41}]_{1\times n} & \Phi_{42} & [\mathbf{\Phi}_{43}]_{1\times n} & \Phi_{44} \end{bmatrix} \tag{7}$$

$$\mathbf{\Phi}^{\mathrm{XT}}_{\mathrm{eq}} = \begin{bmatrix} [\mathbf{\Phi}^{\mathrm{eq}}_{11}]_{n\times n} & [\mathbf{\Phi}^{\mathrm{eq}}_{12}]_{n\times n} \\ [\mathbf{\Phi}^{\mathrm{eq}}_{21}]_{n\times n} & [\mathbf{\Phi}^{\mathrm{eq}}_{22}]_{n\times n} \end{bmatrix} \tag{8}$$

As a result, the entries of matrix $\mathbf{\Phi}_{\rm eq}^{\rm XT}$ are expressed as function of the entries of matrix $\mathbf{\Phi}^{\rm XT}$ as

$$\begin{aligned}
\mathbf{\Phi}_{11}^{\rm eq} &= \mathbf{\Phi}_{11} - (\mathbf{\Phi}_{14} - R_{S0}\mathbf{\Phi}_{12})\,(\mathbf{\Phi}_{21} - R_{SL}\mathbf{\Phi}_{41})\,D^{-1} \\
\mathbf{\Phi}_{12}^{\rm eq} &= \mathbf{\Phi}_{13} - (\mathbf{\Phi}_{14} - R_{S0}\mathbf{\Phi}_{12})\,(\mathbf{\Phi}_{23} - R_{SL}\mathbf{\Phi}_{43})\,D^{-1} \\
\mathbf{\Phi}_{21}^{\rm eq} &= \mathbf{\Phi}_{31} - (\mathbf{\Phi}_{34} - R_{S0}\mathbf{\Phi}_{32})\,(\mathbf{\Phi}_{21} - R_{SL}\mathbf{\Phi}_{41})\,D^{-1} \\
\mathbf{\Phi}_{22}^{\rm eq} &= \mathbf{\Phi}_{33} - (\mathbf{\Phi}_{34} - R_{S0}\mathbf{\Phi}_{32})\,(\mathbf{\Phi}_{23} - R_{SL}\mathbf{\Phi}_{43})\,D^{-1} \qquad (9)
\end{aligned}$$

where: $D = \Phi_{24} - R_{SL}\Phi_{44} - R_{S0}\Phi_{22} + R_{S0}R_{SL}\Phi_{42}$. Hence, XT-induced sources are cast as:

$$\mathbf{V}_{\rm XT0} = -\left(\mathbf{\Phi}_{21}^{\rm eq}\right)^{-1}\mathbf{I}_{\rm XT} \qquad (10)$$

$$\mathbf{V}_{\rm XTL} = -\mathbf{\Phi}_{11}^{\rm eq}\left(\mathbf{\Phi}_{21}^{\rm eq}\right)^{-1}\mathbf{I}_{\rm XT} + \mathbf{V}_{\rm XT} \qquad (11)$$

where vectors $\mathbf{V}_{\rm XT}$, $\mathbf{I}_{\rm XT}$ take the expressions:

$$\begin{aligned}
\mathbf{V}_{\rm XT} &= \left[\mathbf{\Phi}_{12} + (R_{S0}\mathbf{\Phi}_{12} - \mathbf{\Phi}_{14})\,(\Phi_{22} - R_{SL}\Phi_{24})\,D^{-1}\right]V_{S0} \\
&\quad + (\mathbf{\Phi}_{14} - R_{S0}\mathbf{\Phi}_{12})\,D^{-1}V_{SL} \qquad (12) \\
\mathbf{I}_{\rm XT} &= \left[\mathbf{\Phi}_{32} + (R_{S0}\mathbf{\Phi}_{32} - \mathbf{\Phi}_{34})\,(\Phi_{22} - R_{SL}\Phi_{42})\,D^{-1}\right]V_{S0} \\
&\quad + (\mathbf{\Phi}_{34} - R_{S0}\mathbf{\Phi}_{32})\,D^{-1}V_{SL} \qquad (13)
\end{aligned}$$

Eventually, if the XT-induced sources in (10), (11) are expressed as function of V_{S0}, V_{SL} as

$$\mathbf{V}_{\rm XT0} = \boldsymbol{\gamma}_0 V_{S0} + \boldsymbol{\gamma}_{\rm L} V_{SL} \qquad (14)$$

$$\mathbf{V}_{\rm XTL} = \boldsymbol{\delta}_0 V_{S0} + \boldsymbol{\delta}_{\rm L} V_{SL} \qquad (15)$$

where $\gamma_0, \gamma_L, \delta_0, \delta_{\rm L}$ are $n \times 1$ vectors of coefficients satisfying the identifies $\boldsymbol{\gamma_0} = \boldsymbol{\delta}_L = \boldsymbol{\gamma}, \boldsymbol{\gamma}_L = \boldsymbol{\delta_0} = \boldsymbol{\delta}$ due to the symmetry of the XT setup, the unknown open-end voltage sources assuring equivalence between FC and XT are cast as

$$\begin{pmatrix} V_{S0} \\ V_{SL} \end{pmatrix} = \begin{bmatrix} \bar{\gamma} & \bar{\delta} \\ \bar{\delta} & \bar{\gamma} \end{bmatrix}^{-1} \begin{pmatrix} \overline{V}_{\rm FC0} \\ \overline{V}_{\rm FCL} \end{pmatrix} \qquad (16)$$

where $\bar{\gamma}$, $\bar{\delta}$, $\overline{V}_{\rm FC0}$, $\overline{V}_{\rm FCL}$ denote the mean value of the n entries of the corresponding vectors $\boldsymbol{\gamma}$, $\boldsymbol{\delta}$, $\mathbf{V}_{\rm FC0}$, $\mathbf{V}_{\rm FCL}$, respectively.

It is worth noticing here that enforcing equivalence between FC and XT by the feeding conditions in (16) is equivalent to enforce equal CM currents

$$I_{CM}(0) = \frac{1}{n}\sum_{i=1}^{n} I_i(0), \quad I_{CM}(l) = \frac{1}{n}\sum_{i=1}^{n} I_i(l) \qquad (17)$$

in the terminal loads of every wire in the bundle. However, as long as the assumptions introduced in the previous Section are satisfied, the proposed feeding conditions have the potential to assure satisfactory correlation also in terms of currents/voltages induced in the terminations of individual wires in the bundle. Based on this observation, an alternative (simplified) approach exploiting an equivalent representation of the victim harness is proposed in the following Section, which allows enforcing equivalence between FC and XT directly in terms of CM noise induced at the cable ends.

IV. APPROXIMATE CONDITIONS FOR EQUIVALENCE

In this Section, the so-called *Equivalent Cable Bundle* (ECB) method [12]–[14] is applied with the objective to derive a simplified equivalence scheme, assuring approximate equivalence between the CM noise induced by FC and XT in the terminations of the bundle under test.

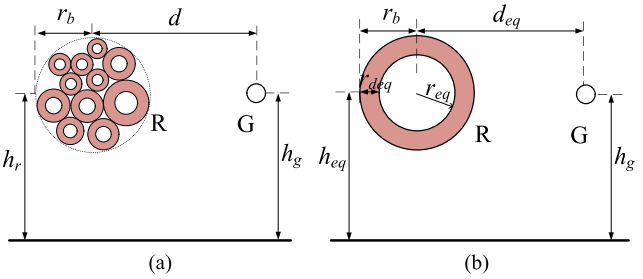

FIGURE 6. Equivalent representation of the XT setup, according to the ECB method: a) Original cross-section, and b) Equivalent cross-section involving the ECB.

A. GEOMETRICAL PARAMETERS OF THE EQUIVALENT BUNDLE

As exemplified in Fig. 6, the basic idea of the ECB method [12], [13] is to substitute the original wiring harness, Fig. 6(a), with an equivalent wire, Fig. 6(b), characterized by equivalent geometrical parameters, that is: height h_{eq}, radius r_{eq}, dielectric thickness r_{deq}, distance from the generator wire d_{eq}.

According to [12], geometrical parameters of the equivalent wire can be expressed as

$$h_{eq} = \frac{1}{n}\sum_{i=1}^{n} h_i \quad d_{eq} = \sqrt{\frac{4h_{eq}h_g}{e^{4\pi L_{gr}/\mu_0}}} \quad r_{eq} = \frac{2h_{eq}}{e^{2\pi L_{rr}/\mu_0}} \qquad (18)$$

where L_{rr} and L_{gr}, i.e., the self- and the mutual inductance of the reduced wire (receptor, subscript "r") with respect to the generator wire (subscript "g"), respectively, are expressed as function of the corresponding self-inductances, L_{jk} for $j = k$, and mutual inductances, L_{jk} for $j \neq k$, of the original structure as

$$L_{gr} = \frac{1}{n}\sum_{j=1}^{n} L_{gj}, \quad L_{rr} = \frac{1}{n^2}\sum_{j=1}^{n}\sum_{k=1}^{n} L_{jk}. \qquad (19)$$

The expressions in (18) and (19) can be further approximated by recalling the filament-bundle condition ($h \gg r_b$) introduced in Section III.C. Accordingly, the height of the equivalent bundle is readily obtained as $h_{eq} = h_r$. Moreover, if such a condition is satisfied in combination with the assumption of weak coupling ($d \gg r_b$), the mutual inductance L_{gr} can be approximated as:

$$L_{gr} = \frac{1}{n}\sum_{j=1}^{n} L_{gj} \approx \frac{\mu_0}{4\pi}\ln\left(\frac{4h^2}{d^2}\right). \qquad (20)$$

Hence, substitution of (20) in (18) yields: $d_{eq} = d$.

Eventually, to evaluate the equivalent radius in (18), the self-inductance L_{rr} of the reduced bundle has to be evaluated

starting from the self and mutual inductances associated with all wires within the bundle. Since the analytical expressions for these quantities, i.e.,

$$L_{jk}\big|_{j\neq k} = \frac{\mu_0}{4\pi}\ln\left(\frac{4h_jh_k}{s_{jk}^2}\right), \quad L_{jk}\big|_{j=k} = \frac{\mu_0}{2\pi}\ln\left(\frac{2h_j}{r_j}\right) \tag{21}$$

exhibit a logarithm dependence on geometrical characteristics, approximate expressions for (21) can be obtained by substituting the involved geometrical parameters with their mean value over all wires in the bundle, that is by: $\bar{h} = h_r$, $\bar{s} = r_b, \bar{r} = (r_{\min}+r_{\max})/2$. Accordingly, the self-inductance L_{rr} can be roughly approximated as:

$$L_{rr} = \frac{1}{n^2}\sum_{j=1}^{n}\sum_{k=1}^{n}L_{jk} \approx \frac{\mu_0}{2\pi}\ln\left[2h\sqrt[n]{\frac{2}{(r_{\min}+r_{\max})r_b^{n-1}}}\right], \tag{22}$$

which leads to the following (approximate) expression of the equivalent wire radius in (18):

$$r_{eq} \approx r_b^{\frac{n-1}{n}}\sqrt[n]{\frac{r_{\min}+r_{\max}}{2}}. \tag{23}$$

Once geometrical characteristics of the equivalent wire are determined (either exploiting the aforesaid approximate expressions, or by direct evaluation of (18), (19) starting from exact values of the involved p.u.l. inductances), the required feeding conditions are those for a single-wire circuit, [6].

B. INFLUENCE OF DIELECTRIC COATING

The above equivalent parameters are derived starting from inductances only, and, as such, they cannot account for the effect due to the dielectric coating surrounding the wires in real harnesses. In this regard, one can observe that the presence of dielectric coating scarcely influences the CM noise induced by FC (actually, only small shifts in the resonant frequencies are observed), and can be therefore neglected in the FC model. This is no longer true as far as XT is considered, since it non-negligibly impacts on capacitive coupling between the wires. In order to (approximately) account for dielectrics, an equivalent dielectric thickness with $r_{deq} = r_b - r_{eq}$ and relative permittivity equal to the original one can be introduced to mimic a uniform charge distribution on the external surface of the bundle. However, despite the introduction of such an equivalent dielectric jacket, the presence of dielectric coating may weaken the accuracy of the XT model, unless inductive coupling were prevailing over capacitive coupling. To minimize such an effect, it is desirable to realize the generator circuit by a bare wire in the approximate equivalence scheme, and to terminate it in low-impedance loads. In practice, this condition is satisfied if the generator is terminated in the 50 Ω input impedance of typical RF sources.

V. NUMERICAL EXAMPLES

In this Section, the proposed methods (implemented in Matlab) are applied to reconstruct by XT the currents induced in the terminal loads of the 19-wire bundles shown in Fig. 7.

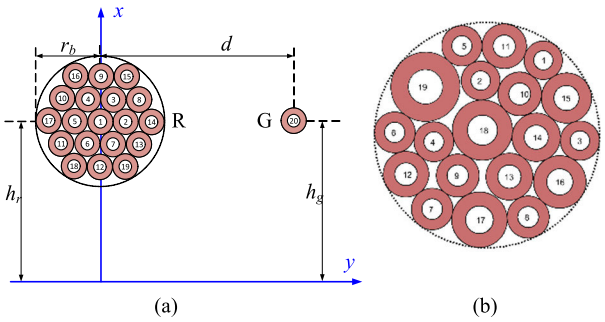

FIGURE 7. (a) Cross section of the XT test setup involving bundle #1; and (b) Cross section (scaled for better readability) of bundle #2.

The first bundle under analysis (hereafter denoted as "bundle #1") exhibits the cross-section in Fig. 7(a), and comprises 19 identical wires of length 0.5 m, radius 1 mm, dielectric thickness 1 mm, and dielectric permittivity 3.5, (hence, the bundle radius results $r_b = 10$ mm). The bundle average height is $h_r = 50$mm, as recommended by EMC standards, [2].

The second bundle under analysis (shown in Fig. (b), and denoted as "bundle #2" in the following) has the same length, geometrical position, and bundle radius r_b of the previous one, but it is composed of wires with different radii. Geometrical characteristics of individual wires in bundle #2 are collected in Tab. 1.

In both test cases, the generator circuit (i.e., wire no. 20) involves a wire with radius 1 mm and length 0.5 m, running at height $h_g = h_r$ above ground, and separated by a distance $d = 50$ mm from the center of the bundle under test, so that both the weak coupling and the filament bundle assumptions are barely satisfied ($h_r = d = 5r_b$). In the proposed validation examples, the generator circuit is realized by exploiting either a bare wire (for the approximate equivalent scheme) or a coated wire (for the exact scheme of equivalence) with dielectric thickness 1 mm, and dielectric permittivity 3.5. The corresponding p.u.l. parameters are calculated by using Ansys Maxwell.

A. VALIDATION OF THE FILAMENT BUNDLE APPROXIMATION

In Section II.C, the filament bundle approximation is introduced to enforce equivalence between FC and XT by means of average feeding conditions. Validity of such an approach is strictly related to the possibility to neglect the differences between the actual entries of FC induced vectors $\mathbf{V_{FC0}}, \mathbf{V_{FCL}}$ in (1) and XT coefficients in the vectors $\boldsymbol{\delta}, \boldsymbol{\gamma}$ in (15), which are inherently assumed to be equal as long as the aforesaid approximation is assumed.

To prove the effectiveness of the proposed approach (which is a prerequisite for the validity of both methods), bundle #1 is considered as the test case, and the entries of vectors $\mathbf{V_{FC0}}$, $\mathbf{V_{FCL}}, \boldsymbol{\delta}, \boldsymbol{\gamma}$ are computed and compared. The obtained results are plotted in Fig. 8 (for FC) and Fig. 9 (for XT). In these figures, each cluster contains 19 curves, corresponding to

TABLE 1. Parameters of individual wires in bundle #2.

Wire no.	1	2	3	4	5	6	7	8	9	10	11	12	13	14	15	16	17	18	19
r_i, r_{di} [mm]	0.9	0.9	0.9	0.9	0.9	0.9	0.9	0.9	0.9	1.0	1.0	1.0	1.0	1.1	1.1	1.2	1.2	1.3	1.5
h_i [mm]	5.0	-0.6	8.2	-4.7	-2.2	-8.2	-4.9	3.7	-2.6	2.9	1.5	-7.2	2.0	4.4	7.0	6.5	-0.7	-0.4	-5.5
y_i [mm]	6.6	4.8	-0.5	-0.6	7.9	0.2	-6.6	-7.3	-3.6	3.6	7.9	-3.5	-3.7	-0.2	3.3	-4.1	-7.5	0.4	4.3
Z_{0i}, Z_{li} [Ω]	1	57	112	168	223	279	334	390	445	501	556	612	667	723	778	834	889	945	1000

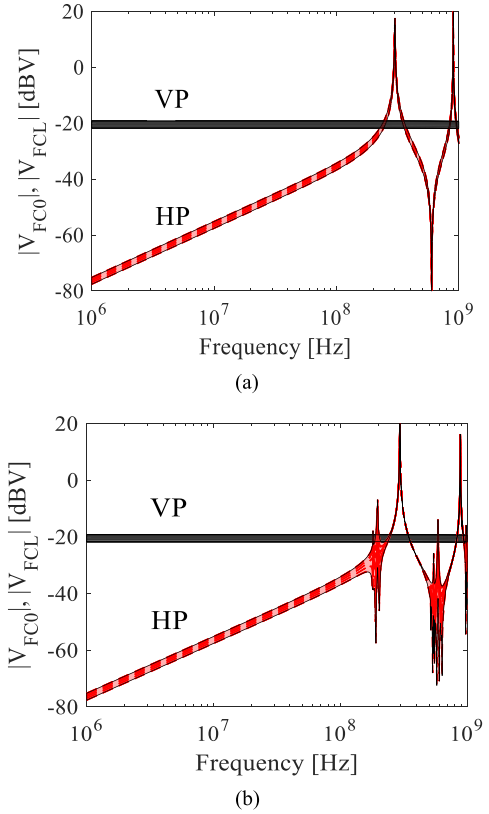

FIGURE 8. Magnitude of FC sources V_{FC0} or V_{FCL} (they satisfy the equality $|V_{FC0}| = |V_{FCL}|$) in (1) for the 19 wires in bundle #1 (a) in the absence, and (b) presence of dielectric coating surrounding the wires.

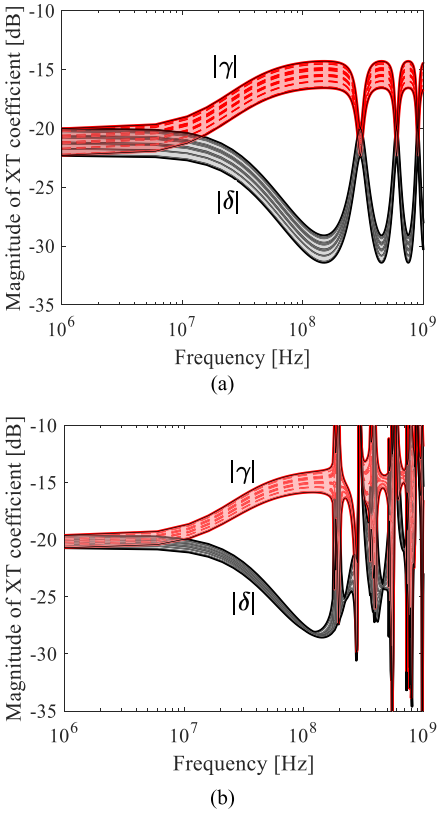

FIGURE 9. Magnitude of XT coefficients in (15) for the 19 wires in bundle #1 (a) in the absence, and (b) presence of dielectric coating surrounding the wires.

the 19 individual wires belonging to the bundle under analysis. Curves in Fig. 8(a) and Fig. 9(a) were evaluated assuming bare wires. Those in Fig. 8(b) and Fig. 9(b) were obtained in the presence of dielectric coating surrounding the wires.

Both in the presence and in the absence of dielectrics, the spread within every cluster of curves is generally limited to a few of decibels (with maximum spread in the order of 2 dB), thus proving the effectiveness of the proposed approximate assumption. In the presence of dielectric coating, the frequencies responses of the crosstalk coefficient and of the sources induced by FC in HP case exhibit additional resonances above 100 MHz, whose occurrence was also proved by full-wave simulation (not shown here for brevity).

In passing, it is worth mentioning here that the relationships between $\mathbf{V_{FC0}}$ and $\mathbf{V_{FCL}}$ derived in [10] in the specific case of a single bare are still valid for individual coated wires in a bundle, since vector entries satisfy the equalities: $\mathbf{V_{FCL}} = \mathbf{V_{FC0}}$ for VP, and $\mathbf{V_{FCL}} = \mathbf{V^*_{FC0}}$ for HP.

B. FEEDING VOLTAGES AND RESONANCES

For the two bundles under analysis, the magnitude of the open-end voltages of the two RF sources connected at the terminations of the generator circuit so to achieve equivalence with FC are plotted in Fig. 10 (bundle #1) and Fig. 11 (bundle #2). Plots in the first row were obtained by the exploiting the first (exact) equivalence scheme, those in the second row by employing the ECB approximation. Furthermore, the feeding conditions in the left panels assure equivalence in the case of VP of the antenna, those in the right panels for HP, and were evaluated both in the presence and in the absence of dielectric coating surrounding the wires. Particularly, owing to the symmetry of the considered incidence conditions as well as of the passive part of the

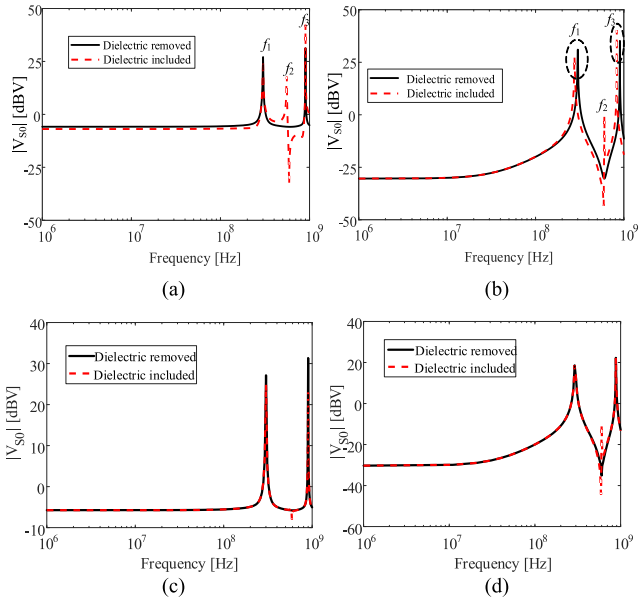

FIGURE 10. Magnitude of $V_{S0} = V_{SL}$ for bundle #1. Exact equivalence scheme: (a) VP and (b) HP. Approximate equivalence scheme: (c) VP and (d) HP.

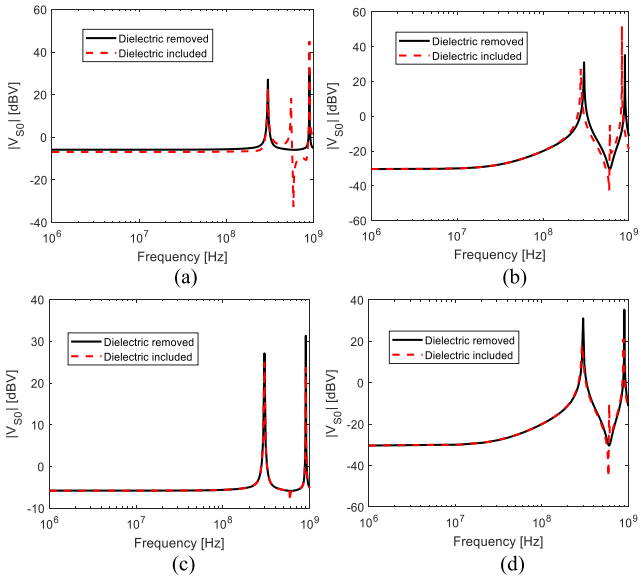

FIGURE 11. Magnitude of $V_{S0} = V_{SL}$ for bundle #2. Exact equivalence scheme: (a) VP and (b) HP. Approximate equivalence scheme: (c) VP and (d) HP.

generator circuit, voltages V_{S0}, V_{SL} are equal in magnitude for both polarizations. Hence, only V_{S0} is plotted in Fig. 10 and Fig. 11.

In the frequency interval under analysis, resonances are observed at frequencies $f_1 = 0.5f_0$, $f_2 = f_0$, and $f_3 = 1.5f_0$, where f_0 denotes the resonant frequency of the wiring structure under analysis. Resonances at frequencies which are integer multiple of f_0(e.g., f_2) only occur in the presence of dielectric coating. At these frequencies, both FC and XT-induced voltages take minimum values. Conversely, resonances occurring at frequencies $(m + 1/2)f_0, m \in \mathbb{N}$ identify frequency points at which FC-induced voltages take maximum values, yet the frequency response of XT-induced voltages exhibit notches. Hence, running the test at those frequencies may require a considerable amount of power to assure equivalence with FC, because of the extremely low coupling efficiency of XT.

C. BUNDLE#1: RECONSTRUCTION OF LOAD CURRENTS

In this Sub-section, the effectiveness of proposed methods is validated for bundle #1. To this end, the generator circuit is driven by the feeding profiles shown in Fig. 12, and the currents induced by XT at the terminations of the bundle under test are compared versus those induced by FC.

In the first test case, whose results are shown in Fig. 12, all wires in the bundle are terminated with 50 Ω impedances, i.e., $Z_{0i} = Z_{li} = 50\ \Omega$. The plots in Fig. 12 compare the CM currents and the currents induced at the terminations of individual wires (namely, a wire was selected for every layer) in the bundle by XT and FC. The proposed results were obtained both for HP (first row) and VP (second row) of the antenna, and in the absence (first column) and in the presence (second column) of dielectric coating surrounding the wires.

Comparing the currents induced on wires belonging to different layers, one can observe the effect of shielding played by the outermost conductors on the internal wires, whose induced current is generally lower.

In terms of induced CM currents, both the exact and approximate equivalence scheme provide accurate reconstruction of the CM current induced by FC. This result is generally confirmed also for individual wires currents, which are satisfactory reconstructed by both the proposed equivalence schemes. Particularly, the most satisfactory results are achieved for the inner wires (e.g., the best matching is obtained for the center wire, i.e., wire no. 1, in this example), since their position in the bundle is closer (than for the outermost wires) to the average position considered to derive the exploited feeding conditions.

To prove the independence of the proposed equivalence schemes on loading conditions, an additional example is here proposed, where the load impedances connected at the terminations of the bundle under test are set as in the last row of Tab. 1. The obtained results are shown in Fig. 13, which further confirm the accuracy of both equivalence schemes in reproducing the noise currents induced at the bundle terminals though FC.

D. BUNDLE #2: RECONSTRUCTION OF LOAD CURRENTS

For the second wire bundle in Fig. 7, load currents induced by FC and those reconstructed by XT by the proposed exact and approximate equivalence schemes are compared in Fig. 14. The results were obtained for the loading conditions collected in Tab. 1. Moreover, simulations were carried out for HP and VP of the antenna (first and second row, respectively), and by exploiting wires without (first column) and with (second column) dielectric coating.

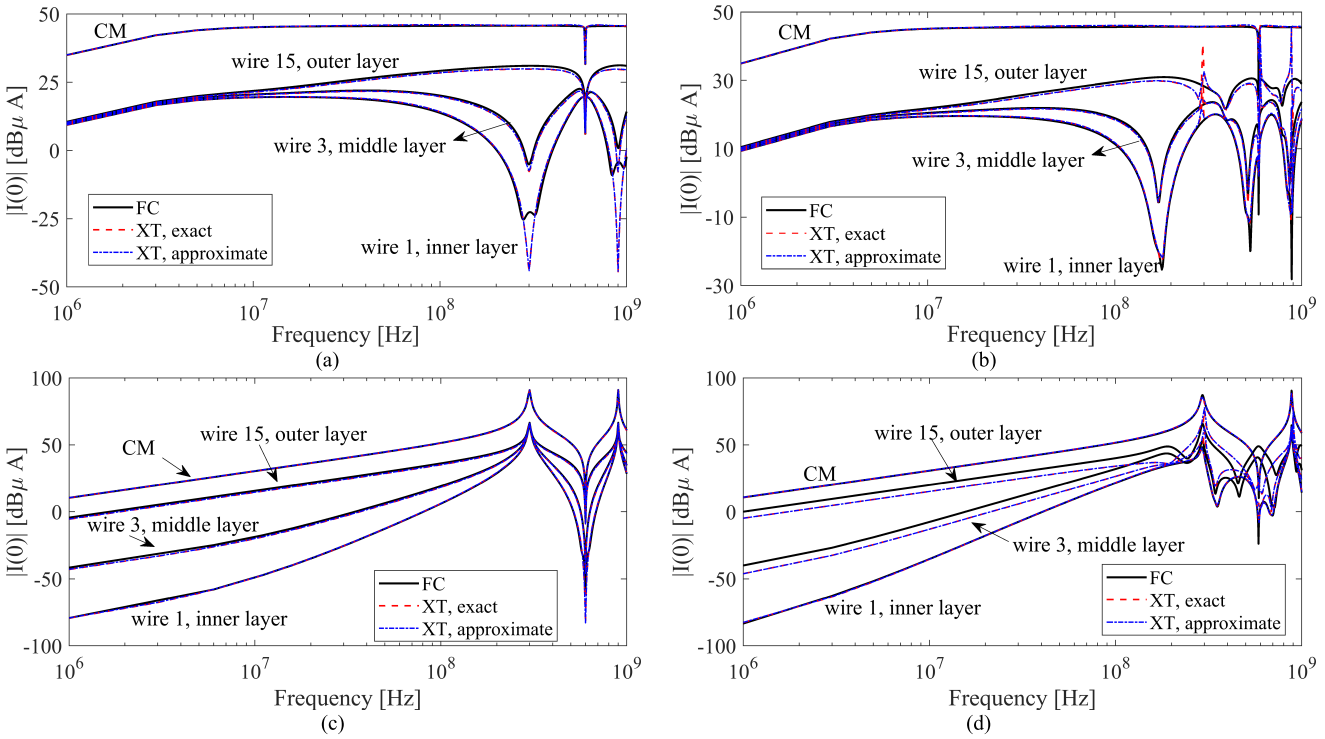

FIGURE 12. Reconstruction by XT of the currents induced by FC at the terminations (50 Ω loads) of bundle #1: (a) HP, bare wires; (b) HP, coated wires; (c) VP, bare wires; (d) VP, coated wires.

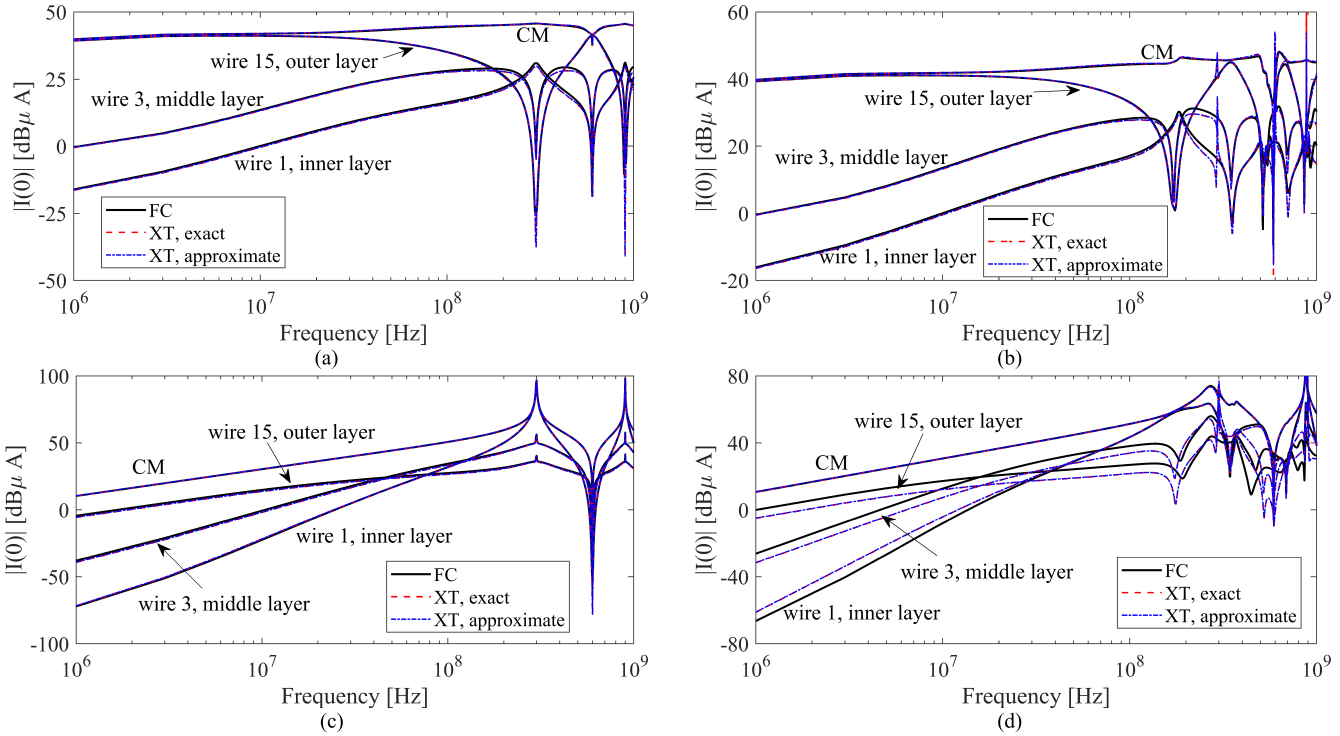

FIGURE 13. Reconstruction by XT of the currents induced by FC at the terminations (loads are as in Tab. 1) of bundle #1: (a) HP, bare wires; (b) HP, coated wires; (c) VP, bare wires; (d) VP, coated wires.

On the whole, a satisfactory agreement is achieved, thus confirming the effectiveness of the proposed schemes of equivalence, especially for the reconstruction of the induced CM current and the currents of individual wires belonging to the inner wires in the bundle. The differences observed for external wires (here wire no. 16) are to be ascribed to the fact

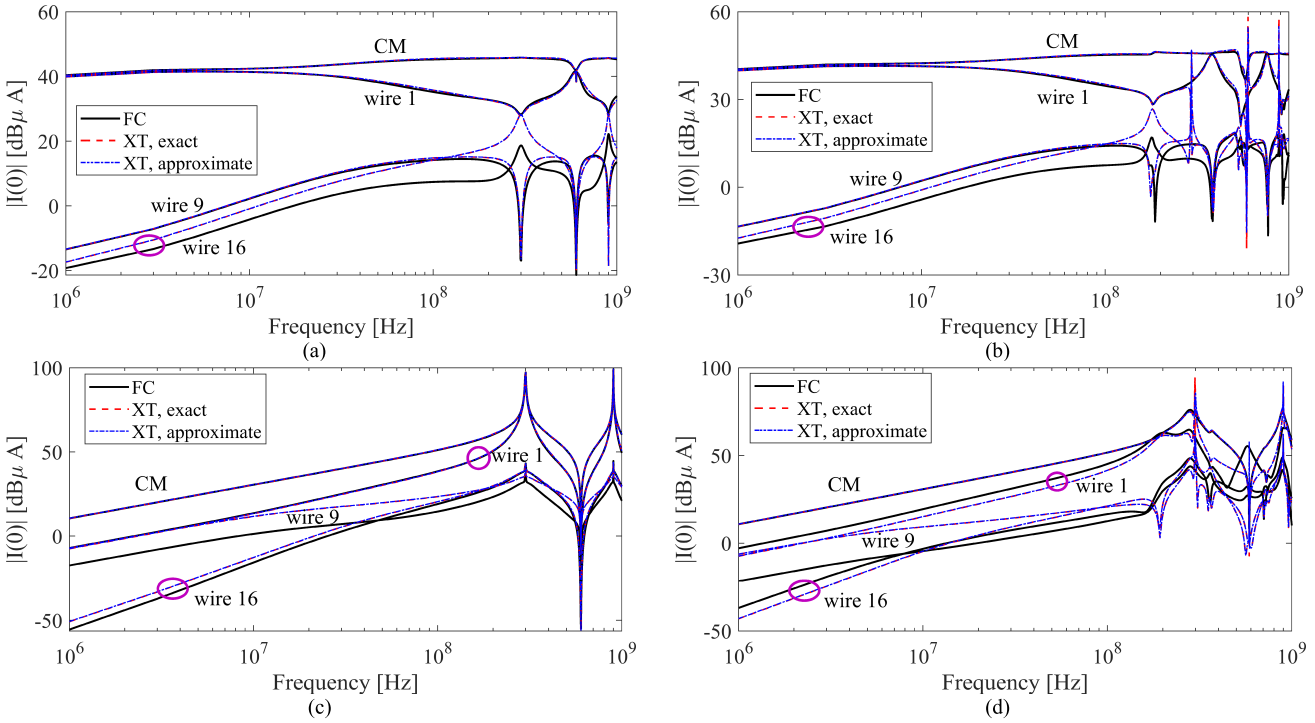

FIGURE 14. Reconstruction by XT of the currents induced by FC at the terminations (loads are as in Tab. 1) of bundle #2: (a) HP, bare wires; (b) HP, coated wires; (c) VP, bare wires; (d) VP, coated wires.

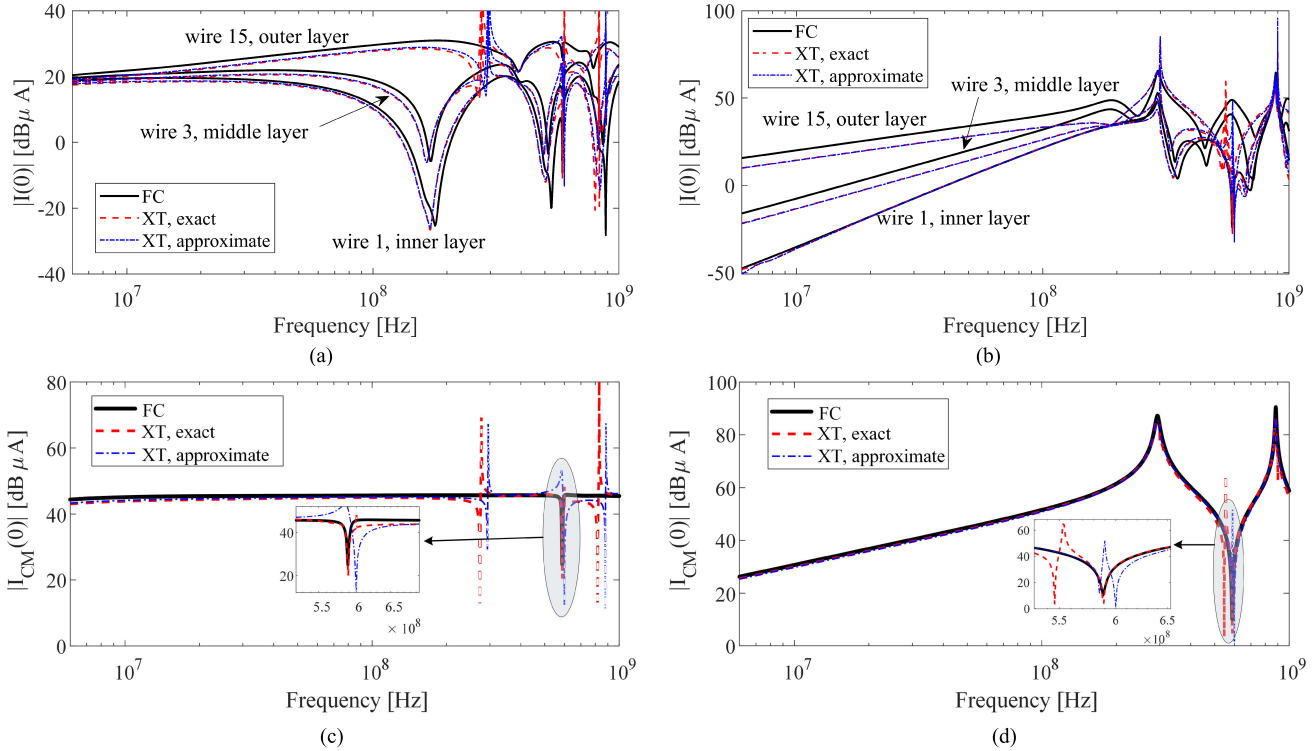

FIGURE 15. Virtual experiments through CST MWS numerical simulation: (a) Currents in individual wires: HP; (b). Currents in individual wires: VP; (c). CM current in the bundle: HP; (d). CM current in the bundle: VP.

that the position of external wires may non-negligibly differ from the average position considered to evaluate the feeding conditions.

Moreover, it can be observed that the inclusion of dielectric coating may involve several spikes in the CM current and on the currents induced on individual wires, which indicates

that exploiting the proposed method at line resonances can be cumbersome, especially when the bundle cross-section exhibits irregularity and randomness in wire positioning.

VI. VIRTUAL EXPERIMENTS

In order to further validate the proposed schemes of equivalence, the XT test setup involving bundle #1 was implemented in the simulation environment CST MWS. Full-wave electromagnetic simulations (FIT solver) were run in the frequency range from 6 MHz up to 1 GHz (to avoid solver accuracy limitation at low frequency), by exploiting the exact and approximate feeding conditions derived in Sec. III and Sec. IV, respectively. The obtained load currents at the bundle terminals were then compared versus those predicted by the FC model in Sec. III.

Examples of obtained results are shown in Fig. 15, where solid curves are the currents induced by FC, whereas dashed-red and dashed-blue curves are the currents induced by XT as computed by the numerical solver by exploiting the exact and approximate conditions of equivalence, respectively.

On the whole, the comparison versus full-wave simulations confirms the ability of the proposed XT-based procedure to accurately reproduce the CM current induced in the bundle under test. A few of spurious resonances are observed especially for HP, which are mainly to be ascribed to TL theory limitation in accounting for high-order propagation modes. As far as the comparison of individual wire currents is concerned, it is confirmed that the test can assure higher accuracy in the reconstruction of the currents induced into the inner wires of the bundle. Indeed, moving far from the bundle center, the observed differences increase since the distance between the axis of a specific wire in the bundle and the average wire position increases.

VII. CONCLUSION

Two formulations of the feeding conditions of the XT test setup were derived to reproduce, in the terminal units of a multiwire bundle, the same currents that would be induced by FC in a RS test setup, overcoming previous works devoted to single bare wire [6], [7], or a differential pairs [8]. The first formulation was derived by MTL theory under weak-coupling and filament-bundle assumptions. The second, approximate formulation was derived by bundle-reduction techniques. Assessment through simulations of a bundle composed of 19 wires, without and with dielectric cover, pointed out strengths and weaknesses of the different equivalence schemes.

Both the formulations lead to a very good reproduction of the comprehensive CM current in the bundle (differences of few dBs are negligible from the viewpoint of industrial RS testing) also in the presence of dielectric coating (practically, the always relevant case). As far as individual currents of wires are concerned, the exact reproduction is inherently not possible for XT. On the other hand, this is true for any other injection method based on a dominant CM-coupling mechanism (for instance BCI method). Anyway, the obtained results show the potential of XT also in the reproduction of these individual currents, especially for the inner wires of the bundle.

The reproduction of FC-induced currents is achieved for arbitrary terminal impedances. Indeed, the feeding conditions of the XT test do not involve properties of the equipment under test connected to cable terminals, which are usually unknown to test operators in most practical conditions. This is the main advantage of the proposed XT test setup with respect to other techniques like BCI, making it a valid alternative for pre-compliance RS investigation in industry.

REFERENCES

[1] *Electromagnetic Compatibility (EMC)-Part 4-3: Testing and Measurement Techniques—Radiated, Radio-Frequency, Electromagnetic Field Immunity Test*, document IEC 61000-4-3, 2010.

[2] *Environmental Conditions and Test Procedures for Airborne Equipment*, document RTCA-DO160 G, Dec. 2014.

[3] *Road vehicles-Component test Methods for Electrical Disturbances from Narrowband Radiated Electromagnetic Energy-Part 2: Absorber-Lined Shielded Enclosure*, document ISO 11452-2, Sep. 2016.

[4] *Reqirements for the Control of Electromagnetic Interference Characteristics of Subsystems and Equipment*, document MIL-STD 461 G, Dec. 2015.

[5] D. A. Hill, "Currents induced on multiconductor transmission lines by radiation and injection," *IEEE Trans. Electromagn. Compat.*, vol. 34, no. 4, pp. 445–450, Nov. 1992.

[6] J. W. Adams, J. Cruz, and D. Melquist, "Comparison measurements of currents induced by radiation and injection," *IEEE Trans. Electromagn. Compat.*, vol. 34, no. 3, pp. 360–362, Aug. 1992.

[7] M. Klingler, M. Szelag, and M. Heddebaut, "Double bulk current injection: A possible substitute to field-to-wire coupling," in *Proc. Eur. Electromagn. Int. Symp. Electromagn. Environ. Consequences*, Bordeaux, France, 1994, pp. 1249–1256.

[8] X. Lu, X. Pan, L. Fan, H. Wan, and G. Wei, "Dual-port pulsed differential-mode current injection method for high-level electromagnetic pulse radiated susceptibility testing," *IET Sci., Meas. Technol.*, vol. 10, no. 5, pp. 505–512, Aug. 2016.

[9] X. Lu, G. Wei, X. Pan, X. Zhou and L. Fan, "A pulsed differential-mode current injection method for electromagnetic pulse field susceptibility assessment of antenna systems," *IEEE Trans. Electromagn. Compat.*, vol. 57, no. 6, pp. 1435–1446, 2015.

[10] F. Grassi, H. Abdollahi, G. Spadacini, S. A. Pignari, and P. Pelissou, "Radiated immunity test involving crosstalk and enforcing equivalence with Field-to-Wire coupling," *IEEE Trans. Electromagn. Compat.*, vol. 58, no. 1, pp. 66–74, Feb. 2016.

[11] K. Yuan, F. Grassi, G. Spadacini, and S. A. Pignari, "Reproducing field-to-Wire coupling effects in twisted-wire pairs by crosstalk," *IEEE Trans. Electromagn. Compat.*, vol. 60, no. 4, pp. 991–1000, Aug. 2018.

[12] G. Andrieu, L. Koná, F. Bocquet, B. Dámoulin, and J.-P. Parmantier, "Multiconductor reduction technique for modeling common-mode currents on cable bundles at high frequency for automotive applications," *IEEE Trans. Electromagn. Compat.*, vol. 50, no. 1, pp. 175–184, Feb. 2008.

[13] G. Andrieu, A. Reineix, X. Bunlon, J.-P. Parmantier, L. KonÉ, and B. DÉmoulin, "Extension of the equivalent cable bundle method for modeling electromagnetic emissions of complex cable bundles," *IEEE Trans. Electromagn. Compat.*, vol. 51, no. 1, pp. 108–118, Feb. 2009.

[14] B. Schetelig, J. Keghie, R. Kanyou Nana, L.-O. Fichte, S. Potthast, and S. Dickmann, "Simplified modeling of EM field coupling to complex cable bundles," *Adv. Radio Sci.*, vol. 8, pp. 211–217, Oct. 2010.

[15] C. R. Paul, *Analysis of Multiconductor Transmission Lines*. New York, NY, USA: Wiley, 2008.

[16] F. Rachidi, "A review of Field-to-Transmission line coupling models with special emphasis to lightning-induced voltages on overhead lines," *IEEE Trans. Electromagn. Compat.*, vol. 54, no. 4, pp. 898–911, Aug. 2012.

[17] S. Pignari and F. G. Canavero, "Theoretical assessment of bulk current injection versus radiation," *IEEE Trans. Electromagn. Compat.*, vol. 38, no. 3, pp. 469–477, Aug. 1996.

TAO LIANG (Member, IEEE) received the B.Sc. degree in electrical engineering and automation from Xi'an Jiaotong University, Shaanxi, China, in 2013, the double M.Sc. degrees in electrical engineering from Xi'an Jiaotong University and the Politecnico di Milano, Milan, Italy, in 2016, and the Ph.D. degree *(summa cum laude)* in electrical engineering from the Politecnico di Milano, in 2019.

He is currently with the School of Electrical Engineering, Xi'an Jiaotong University. His research interests include electromagnetic compatibility (EMC) modeling and testing techniques.

XINGLONG WU (Graduate Student Member, IEEE) received the double M.Sc. degrees in electrical engineering (EE) from Xi'an Jiaotong University, Xi'an, China, and the Politecnico di Milano, Milan, Italy, in 2015, and the Ph.D. degree *(summa cum laude)* in EE from the Politecnico di Milano, in 2019.

In March 2017 and June 2017, he was a Visiting Scientist with the Electromagnetics Group, Department of Information Technology, Ghent University, Belgium. He is currently a Postdoctoral Research Fellow with the Department of the Electronics, Information and Bioengineering, Politecnico di Milano. His research interests include distributed parameter circuit modeling, statistical techniques for electromagnetic compatibility (EMC), and system-level EMC.

FLAVIA GRASSI (Senior Member, IEEE) received the Laurea (M.Sc.) and Ph.D. degrees in electrical engineering from the Politecnico di Milano, Milan, Italy, in 2002 and 2006, respectively.

From 2008 to 2009, she was a Research Fellow with the European Space Agency (ESA), ESA/ESTEC, The Netherlands. She is currently an Associate Professor with the Department of Electronics, Information and Bioengineering, Politecnico di Milano. Her research interests include distributed-parameter circuit modeling, statistical techniques, characterization of measurement setups for EMC testing (aerospace and automotive sectors), and application of the power line communications technology in ac and dc lines.

Dr. Grassi received the International Union of Radio Science (URSI) Young Scientist Award, in 2008, the IEEE Young Scientist Award at the 2016 Asia–Pacific International Symposium on EMC (APEMC), the IEEE EMC Society 2016 Transactions Prize Paper Award, and the Best Symposium Paper Award at the 2015 and 2018 APEMC.

GIORDANO SPADACINI (Senior Member, IEEE) received the Laurea (M.Sc.) and Ph.D. degrees in electrical engineering from the Politecnico di Milano, Italy, in 2001 and 2005, respectively.

He is currently an Associate Professor with the Department of Electronics, Information and Bioengineering, Politecnico di Milano. His research interests include statistical models for the characterization of interference effects, distributed parameter circuit modeling, experimental procedures and setups for EMC testing, and EMC in aerospace, automotive, and railway systems. He was a recipient of the 2005 EMC Transactions Prize Paper Award, the 2016 Richard B. Schulz Best EMC Transactions Paper Award, and the Best Symposium Paper Awards from the 2015 Asia-Pacific International Symposium on EMC (APEMC) and the 2018 Joint IEEE EMC and APEMC Symposium.

SERGIO AMEDEO PIGNARI (Fellow, IEEE) received the Laurea (M.S.) and Ph.D. degrees in electronic engineering from the Politecnico di Torino, Turin, Italy, in 1988 and 1993, respectively.

From 1991 to 1998, he was an Assistant Professor with the Department of Electronics, Politecnico di Torino. In 1998, he joined the Politecnico di Milano, Milan, Italy, where he is currently a Full Professor of the Circuit Theory and Electromagnetic Compatibility (EMC) at the Department of Electronics, Information, and Bioengineering, and the Chair of the Board of B.Sc. and M.Sc. Study Programmes in electrical engineering, from 2015 to 2020. He was a member of the International Academic Committee with the State Key Laboratory of Electrical Insulation and Power Equipment (SKLEIPE), Xi'an Jiaotong University (XJTU), Xi'an, China, from 2015 to 2020. He is the author or coauthor of more than 200 papers published in international journals and conference proceedings. His research interests include EMC and include field-to-wire coupling and crosstalk, conducted immunity and emissions in multiwire structures, statistical techniques for EMC prediction, and experimental procedures and setups for EMC testing.

Dr. Pignari has been a member of the Technical Program Committee of the Asia Pacific EMC Week, since 2010. He was a co-recipient of the 2005 and 2016 IEEE EMC Society Transactions Prize Paper Award, and the 2011 IEEE EMC Society Technical Achievement Award. From 2010 to 2015, he has served as the IEEE EMC Society Chapter Coordinator. From 2007 to 2009, he was the Chair of the IEEE Italy Section EMC Society Chapter. He has been the Technical Program Chair of the ESA Workshop on Aerospace EMC, since 2009. He is serving as an Associate Editor for the IEEE TRANSACTIONS ON ELECTROMAGNETIC COMPATIBILITY.